Electronic Supplementary Material (ESI) for Chemical Science.

Updated 18/01/2022

Supporting Information
(Computational Details)

Divergent Stereochemical Outcomes in the Insertion of Donor/Donor Carbenes into the C–H Bonds of Stereogenic Centers

*Sarah N. Dishman, Croix J. Laconsay, James C. Fettinger, Dean J. Tantillo, and Jared T. Shaw**

Department of Chemistry, University of California, One Shields Ave, Davis, CA, 95616

Computational Details

Computational Methods. Density functional theory (DFT) calculations were carried out using the *Gaussian 16* suite of programs.[1] DFT methods were chosen because of the size of the molecules involved in this study and their reliability to perform well in similar mechanistic studies. DFT methods (similar to those used here) have been successfully implemented in past computational mechanistic studies of C-H insertion reactions of dirhodium carbenes and other transition-metal catalyzed reactions in the field of homogeneous catalysis.[2–7] Geometries of transition state structures (TSSs) and minima along the reaction pathway were optimized using the B3LYP[8] functional with Grimme's D3 correction with Becke-Johnson (BJ) damping (i.e., B3LYP-D3(BJ)) to correct for the lack of dispersion treatment in B3LYP alone.[9,10] Harmonic vibrational frequencies were computed at the same level, from which we extracted free energy correction values (*vide infra*) to compute relative free energies (ΔG); imaginary vibrational modes were visualized to confirm we identified true TSSs; one imaginary frequency confirmed we computed first-order saddle points for TSSs and the lack of any imaginary frequencies confirmed we computed energy minima. Intrinsic reaction coordinate (IRC) calculations were carried out from each TSS to identify flanking minima on the potential energy surface.[11–13]

All computations were carried out with an ultrafine integration grid (99 radial shells and 590 angular points per shell), the default in *Gaussian 16* and recommended minimum-sized integration grid to achieve quantitative accuracy.[14] We employed a Pople-type double-ζ basis set, 6-31G(d) basis set[15] for C, H, O, and N and the LANL2DZ[16] basis set and effective core potential (ECP) for Rh (i.e., B3LYP-D3(BJ)/LANL2DZ[6-31G(d)]) for geometry optimizations. Single-point calculations were subsequently carried out on the above-mentioned optimized geometries with the same functional, B3LYP-D3(BJ), using a larger, more flexible basis set and ECP—the Stuttgart/Dresden SDD ECP[17] for Rh, and 6-31+G(d,p) for C, H, O, and N, which includes diffuse and polarization functions—to more-accurately account for the charged-minima and TSSs in this reaction (i.e., PCM(CH_2Cl_2)-B3LYP-D3(BJ)/SDD[6-31+G(d,p)]//PCM(CH_2Cl_2)-B3LYP-D3(BJ)/LANL2DZ[6-31G(d)]).[18] We observed that increasing the basis set size from double-ζ to triple-ζ (i.e., 6-31G to 6-311G) was too costly to be practical given the size of

the system studied here and the computational resources at our disposal. Adding additional diffuse and/or polarization basis functions, too, can be harmful—not to mention increase the cost—so we reasoned that a minimally-augmented 6-31+G(d,p) basis set would suffice.[19]

All optimized structure coordinates are reported on the ioChem-BD database for ease of access.[20] The reader may find these structures at the following DOI: https://doi.org/10.19061/iochem-bd-6-94

Discussion.

Key Conclusions and Takeaways

The robustness of our chosen level of theory was tested by employing a series of various functionals and computing the $\Delta\Delta E^{\ddagger}$ for TSS's **TS-6b** and **TS-6a** (Table S1). Different functionals achieved varying quantitative results in predicting $\Delta\Delta E^{\ddagger}$'s—the free energy differences fall within ~1-2 kcal/mol, all within typical DFT error. This suggests that we are unable to accurately predict the experimentally observed diastereoselectivity with our employed DFT methods. *However, these results do not diminish the validity and value of our main conclusions that the C-H insertion mechanisms with R-PTAD catalyst is stepwise.* After all, the conclusions drawn from our studies are qualitative, not quantitative.

The key advance that emerges out of our computational studies regards the nature of the bond-making and –breaking events in the C-H insertions event: that the C-H insertion event involves a formally stepwise mechanism with hydride transfer-S_E2 C-C bond formation events. S_E2 mechanisms are unusual and sparsely reported in the literature; as far as we know, they have not been reported for systems involving Rh. Electrophilic cleavages of organomercurial compounds usually exhibit S_E2 retention of configuration at carbon mechanisms; while S_E2 inversion has been reported for some organotin compounds, it is much more rare (at least as far as we know).[21] Concerted (sometimes asynchronous) C-H insertion mechanisms have been invoked frequently for donor/acceptor and acceptor carbenes and these have involved retention of configuration at the C-H insertion carbon, but previously-reported intramolecular C-H insertions with

donor/donor carbenes catalyzed by $Rh_2(OAc)_4$ also involve *stepwise* mechanisms. All of these mechanistic possibilities for hydride shift and C-C bond closure events are depicted on a More O'Ferrall-Jencks plot[22,23] of the sort shown in **SI Figure 3**.[24,25] The stepwise mechanism we report exists very close to (but not within) the border area (light blue) of concerted, and we suspect that this is the case due to the distortion the substrate must adopt in the chiral catalyst cavity (and this distortion may even be *stronger* with inclusion of adamantane groups at the methyl positions where we needed to truncate our *R*-PTAD catalyst model due to computational cost). We hope that future work may validate this claim.

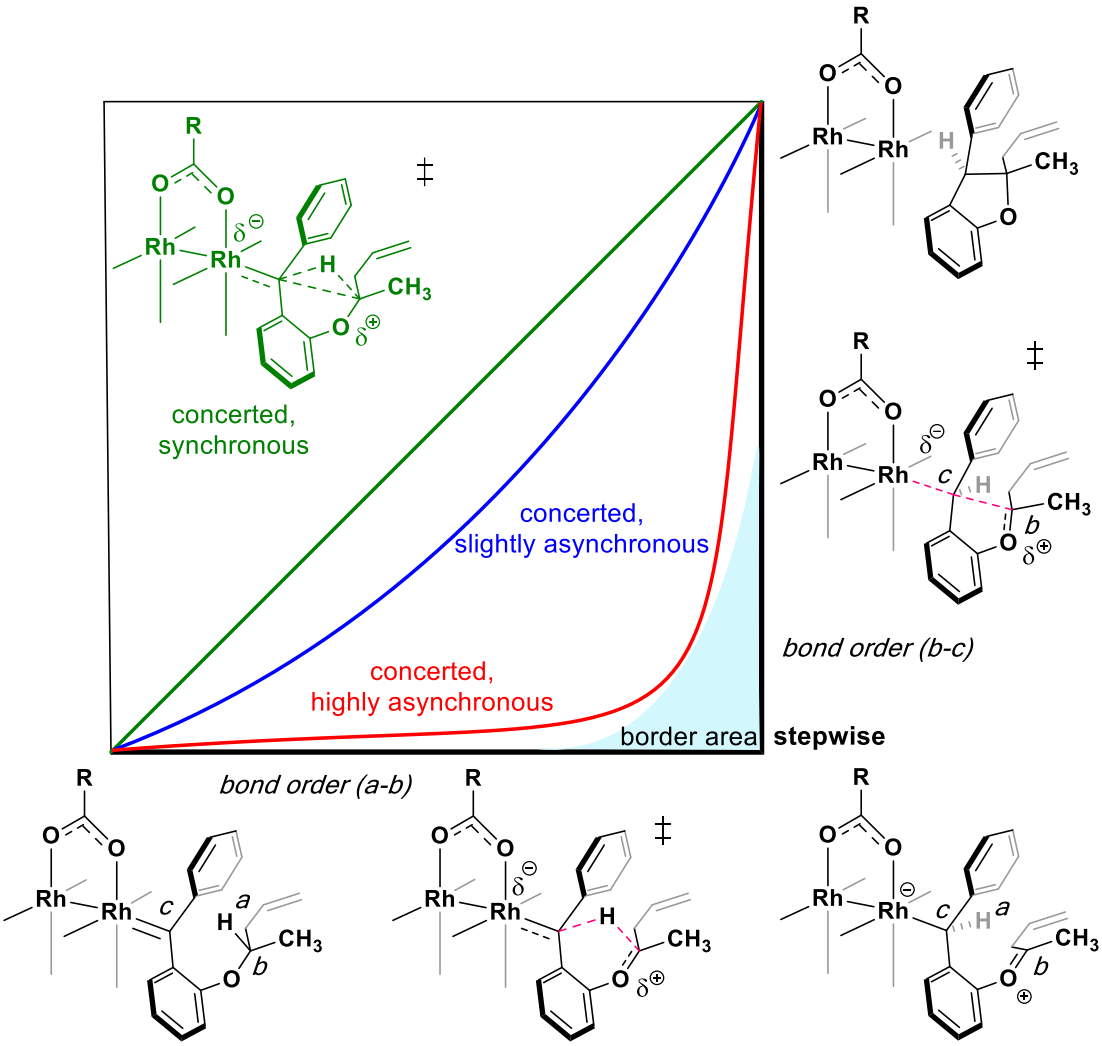

SI Figure 3. Qualitative More O'Ferrall-Jencks plot for Rh-catalyzed C-H insertion of donor/donor carbenes. Past studies have either found clearly stepwise or concerted asynchronous mechanisms, whereas the mechanism discovered here borders the two.

Notable Limitations

That our current model is limited with respect to the origin of diastereoselectivity presents ample opportunity for future experimental and/or theoretical studies to update the current model. Variations in energies emerging out of the DFT functionals in Table S1 leave the origin of diastereoselectivity hanging in the balance and suggests that the use of much higher levels of theory and/or running dynamics simulations—an as-yet impractical task with currently available tools given the size of the system studied here—might aid in future studies.

The relatively flat surface connecting the hydride-shift and S_E2 TSSs on the PES also indicates caution when drawing conclusions based solely on stationary point analysis: plenty of literature discusses that dynamic effects can govern selectivity of reactive species on broad plateau-like regions of potential energy surfaces (PESs).[26] Our model may be further updated by considering the effects of explicit solvent. As we mentioned above, truncating the catalyst may have had a significant effect on the chiral cavity shape, which poses an additional limitation on our model, but we do not believe this compromises the evidence in favor of a stepwise mechanism. So, we are left with a "thin" mechanistic model, which is still valuable for the purposes of this study.[27]

In sum, we have gathered strong evidence that supports a stepwise C-H insertion mechanism.[28] Though the qualitative structure of our mechanism is championed by our results, the *details* about the origin of diastereoselectivity remain elusive. These limitations, however, should inspire future experimental or computational studies. We foresee in the future *ab initio* molecular dynamics and/or a fuller treatment of explicit solvent effects elucidating a clearer origin of stereoselectivity.

Performance of Functionals and Basis Sets, Energies, and Frequencies

Table S1. Single-point energy comparison of $\Delta\Delta E^{\ddagger}$ with various DFT functionals. $\Delta\Delta E^{\ddagger}$'s are computed as the difference between **TS-6b** and **TS-6a**. All single-points were carried out with the SDD basis set and ECP for Rh and 6-31+G(d,p) for all other atoms, unless stated otherwise (in one case we employ the def2-SVP basis set). Single-point calculations were computed at the B3LYP-D3(BJ)/LANL2DZ[6-31G(d)]-optimized geometry.

Functional	$\Delta\Delta E^{\ddagger}$ (kcal mol^{-1})
B3LYP-D3(BJ)	1.1
B3LYP-D3(BJ)/def2-SVP	0.3
PW6B95-D3(BJ)	-0.1
wB97X-D	0.2
PBE0-D3	0.1
M06-D3	-0.6
M06	-0.4
MN15	-1.2

Table S2. Energies and lowest frequencies for structures reported in main text (PCM-(CH_2Cl_2)-B3LYP-D3(BJ)/SDD[6-31+G(d,p)]//PCM(CH_2Cl_2)-B3LYP-D3(BJ)/LANL2DZ[6-31G(d)]). Structure files reported below have been uploaded to ioChem-BD computational chemistry results repository.[20] See the following DOI for structures (included coordinates) for each file name: https://doi.org/10.19061/iochem-bd-6-94

Structure and File Name	**Electronic Energy (Hartree)[a]**	**Free Energy Correction (Hartree)[b]**	**Lowest Frequencies (cm^{-1})**
Rh_RPTAD	-3340.516422	0.6195	8.9
7	-881.5497442	0.269887	25.8
11	-4222.095811	0.921565	11.0
TS-8	-4222.086415	0.919567	-457.7
8	-4112.599943	0.915646	17.2
TS-9	-4112.576339	0.913306	-666.9
9	-4112.579226	0.915079	11.9
10	-4112.581325	0.915125	17.2
TS-6a	-4112.578749	0.915002	-260.5
TS-6b	-4112.57698	0.91628	-202.9
6a	-4112.654441	0.921153	16.7

6b	-4112.656318	0.918993	13.5
SI-22	-4222.09567	0.924957	16.1
SI-TS-23	-4222.083163	0.923123	-444.6
SI-23	-4112.592847	0.914711	12.7
SI-TS-24	-4112.576261	0.910947	-652.7
SI-24	-4112.58106	0.91548	15.4
SI-TS-6b$_{enan}$	-4112.576102	0.913293	-77.0
SI-6b$_{enan}$	-4112.644575	0.914162	11.6
SI-25	-4112.579978	0.914734	9.8

[a] Electronic energies computed at PCM(CH_2Cl_2)-B3LYP-D3(BJ)/SDD[6-31+G(d,p)]//PCM(CH_2Cl_2)-B3LYP-D3(BJ)/LANL2DZ[6-31G(d)] level of theory.
[b] Free energy correction computed at PCM(CH_2Cl_2)-B3LYP-D3(BJ)/LANL2DZ[6-31G(d)] level of theory.

Table S3. Absolute free energies and lowest frequencies for structures reported in **SI Figure 8** (see below). Geometry and frequency calculations were computed at the CPCM(CH_2Cl_2)-B3LYP-D3(BJ)/LANL2DZ[6-31G(d)] level.

Structure and File Name	**Sum of Electronic and Free Energies (Hartree)**	**Lowest Frequencies (cm^{-1})**
A-SM	-2019.096198	16.43
A-TSS1	-2019.083461	-697.51
A-INT	-2019.088658	11.96
A-TSS2	-2019.087938	-123.83
A-P	-886.120479	25.38
A-Cat	-1133.045429	36.75

Potential Energy Surfaces, IRC, and Scans

The potential energy surfaces (PESs) below, SI Figures 4 and 5, provide supporting evidence for a stepwise C-H insertion mechanism in formation of products **6a**, **6b**, **SI-6a$_{enan}$**, and **SI-6b$_{enan}$**. The observed experimental product from the main-text (see Table 2) when **2** is subjected to *R*-3 (entry 4) is **6a** in high dr and er. That the barrier from intermediate **9** to form **6a** (**TS-6a**) is much lower than **TS-6b** in SI Figure S4 supports these data. Though we could not identify a transition state structure (TSS) from **9** to **10**—locating a C_{aryl}-O bond rotation barrier in a large dirhodium complex cavity with a multitude of interactions remained futile after countless attempts—the differences in relative free energies between **TS-6a** and **TS-6b** clearly show **TS-6a** is the favored kinetic exit channel.

SI Figure 5 displays the results of the PES for formation of the enantiomers of the diastereomers that are unfavored. Careful inspection of the relative energies between SI Figures S4 and S5 reveals that the relative barriers for the elementary steps in SI Figure S5 are generally all higher than those in SI Figure S4. What is more, though **8** and **SI-23** look like the same structure—and thus have the same 2D depiction—in the chiral cavity of the (*R*)-catalyst, they are atropisomers of each other due to the diaryl rings (see R. Costil *et al*.[28] for an example of how atropisomerism arises out of diaryl systems), which results in formation of an (*E*)-**9** or (*Z*)-**SI-24** oxocarbenium ion, respectively. Finally, **SI-TS-23**, SI-**TS-6a$_{enan}$** and **SI-TS-6b$_{enan}$** in SI Figure S5 have higher relative energies than **TS-8**, **TS-6a** and **TS-6b**, which all points to toward a theoretical prediction that formation of **6a** should predominate formation of **6b** and their enantiomers, all consistent with what is observed experimentally in the diastereomeric and enantiomeric ratios of Table 2, entry 4 of the main text.

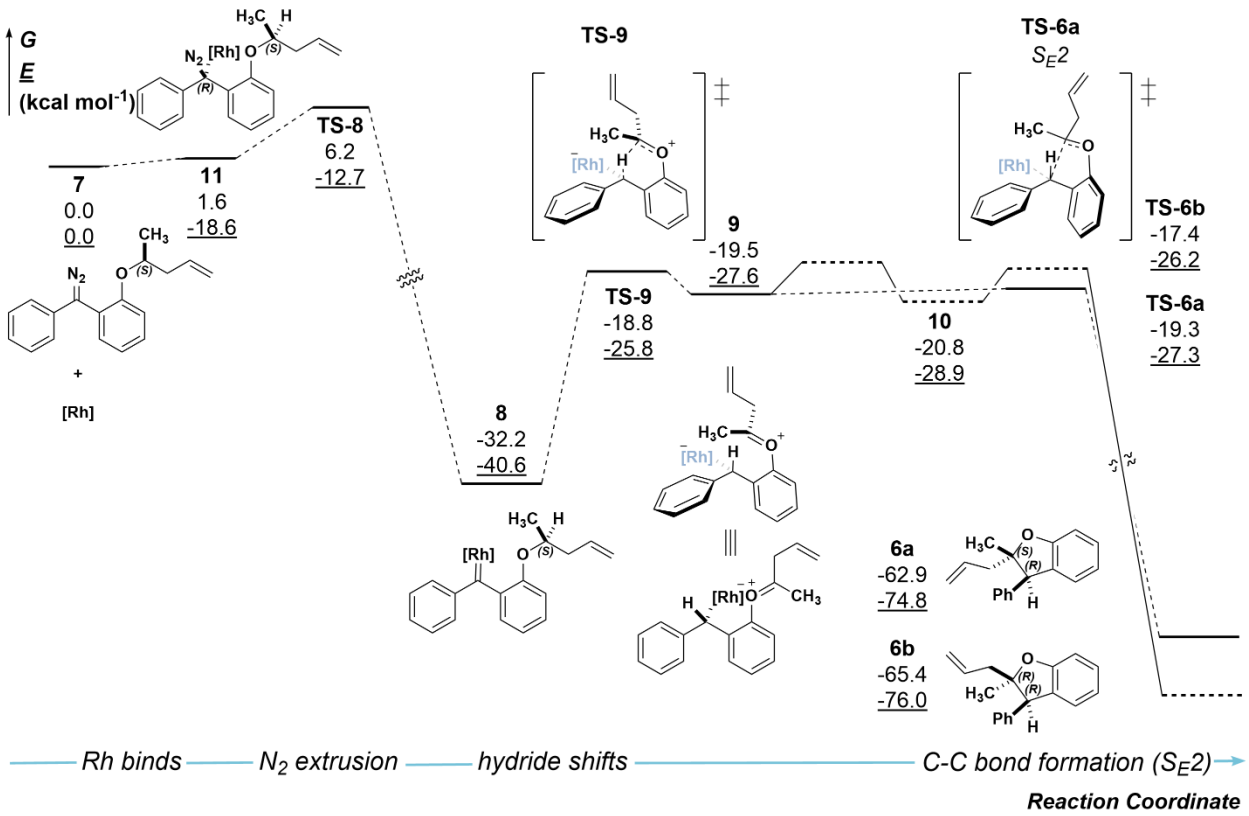

SI Figure 4. Full potential energy surface (PCM(CH_2Cl_2)-B3LYP-D3(BJ)/SDD[6-31+G(d,p)]//PCM(CH_2Cl_2)-B3LYP-D3(BJ)/LANL2DZ[6-31G(d)]) diagram with Rh_2(*R*-PTAD)$_4$ for formation of **6a** and **6b**. Free energies and electronic energies (<u>underlined</u>) are both shown in kcal mol^{-1}.

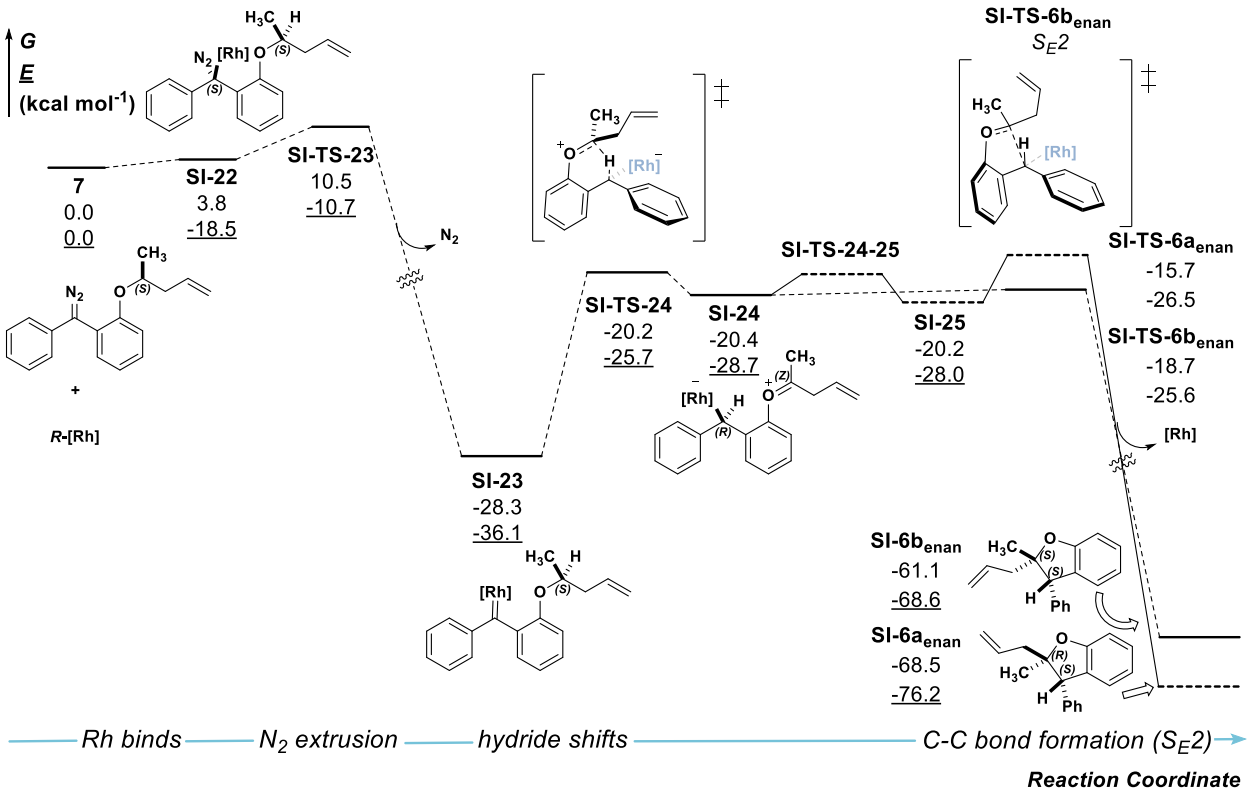

SI Figure 5. Full potential energy surface ((PCM(CH_2Cl_2)-B3LYP-D3(BJ)/SDD[6-31+G(d,p)]//PCM(CH_2Cl_2)-B3LYP-D3(BJ)/LANL2DZ[6-31G(d)]) diagram with Rh_2(*R*-PTAD)$_4$ for formation of **SI-6a$_{enan}$** and **SI-6b$_{enan}$**. Free energies and electronic energies (underlined) are both shown in kcal mol^{-1}.

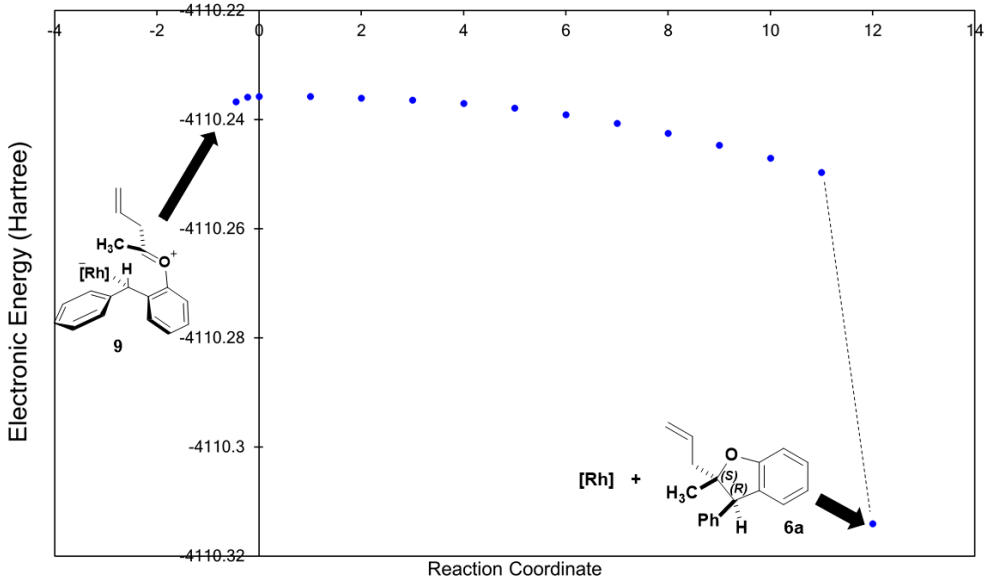

SI Figure 6. Representative intrinsic reaction coordinate (IRC) for TS-6a. The "0" coordinate on the IRC (x-axis) denotes the location of the TSS; intermediate **9** is close in structure to TS-6a and C-C bond formation is highly exergonic. This IRC confirms that TS-6a connects **9** to **6a**. Similar IRC calculations were carried out on all TSSs to confirm they indeed led to flanking minima.

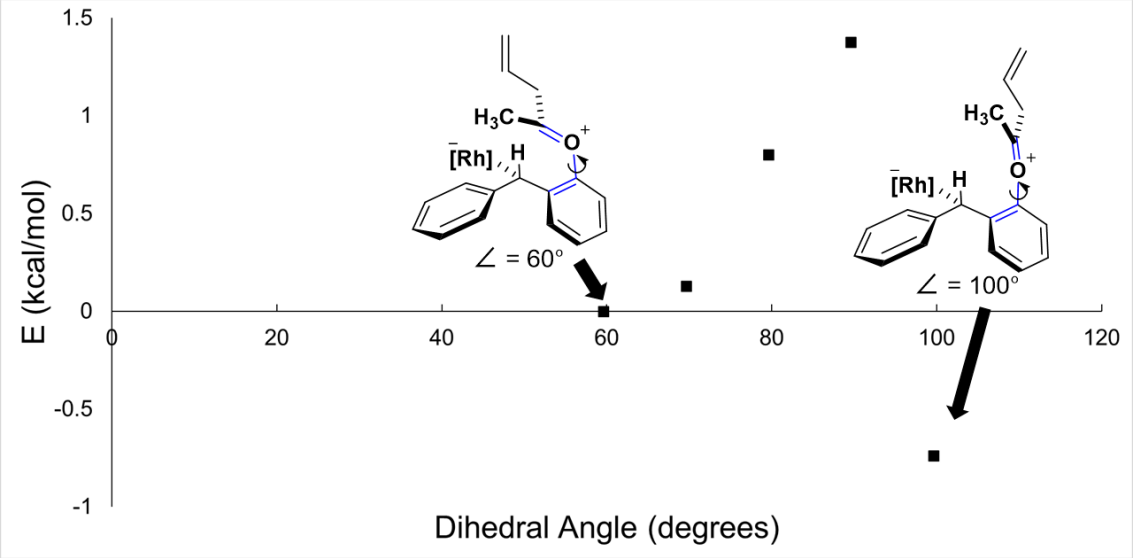

SI Figure 7. Potential energy surface for stereochemical scrambling from **9** to **10**. Based on these results, we observe rotation about the C_{aryl}-O bond (highlighted by the dihedral angle in blue) is higher in potential energy (~1.4 kcal mol^{-1} versus 0.3 kcal mol^{-1}) but not high enough to ignore. A barrier of ~1.4 kcal mol^{-1} to convert **9** to **10** reflects a dr of 86:14 in favor of **6a** with some **6b** diastereomer.

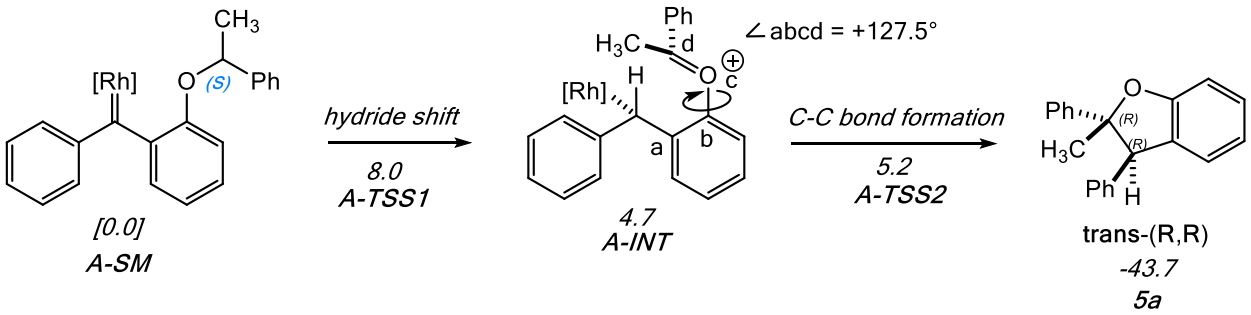

SI Figure 8. Relative free energy (kcal mol^{-1}, CPCM(CH_2Cl_2)-B3LYP/LANL2DZ[6-31G(d)]) profile for formation of **5a** demonstrates the mechanism is stepwise. [Rh] = $Rh_2(OAc)_4$.

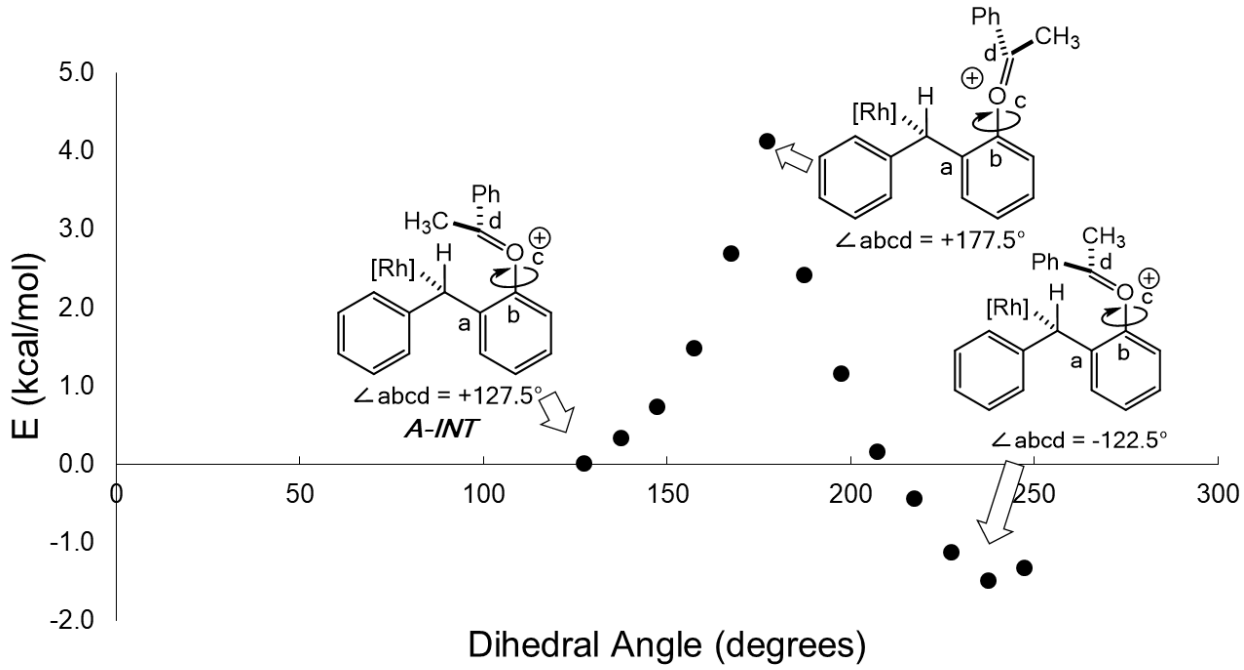

SI Figure 9. The data from the plot indicate that with dirhodium tetraacetate, rotation about the b-c bond in ***A-INT*** requires more energy than to close the ring by a C-C bond formation, approximately greater than 4 kcal/mol for rotation versus 0.5 kcal/mol to close the ring. Though this energy scan only yields relative electronic energies, not free energies as in SI Figure 8, we believe it provides sufficient evidence to suggest that bond rotation for R= Ph, even in the case of an achiral catalyst, costs a greater energetic penalty than forming the product. We suspect that in the chiral cavity of Rh_2(R/S-PTAD)$_4$, this energetic penalty will go up due to significant steric effects between the phthalimide arms of the catalyst and the Ph ring.

References

(1) Frisch, M. J.; Trucks, G. W.; Schlegel, H. B.; Scuseria, G. E.; Robb, M. A.; Cheeseman, J. R.; Scalmani, G.; Barone, V.; Petersson, G. A.; Nakatsuji, H.; et al. Gaussian 16, Revision C.01. Gaussian, Inc.: Willingford, CT 2016.

(2) Pidko, E. A. Toward the Balance between the Reductionist and Systems Approaches in Computational Catalysis: Model versus Method Accuracy for the Description of Catalytic Systems. *ACS Catal.* **2017**, *7* (7), 4230–4234.

(3) Vogiatzis, K. D.; Polynski, M. V.; Kirkland, J. K.; Townsend, J.; Hashemi, A.; Liu, C.; Pidko, E. A. Computational Approach to Molecular Catalysis by 3d Transition Metals: Challenges and Opportunities. *Chem. Rev.* **2019**, *119* (4), 2453–2523.

(4) Sperger, T.; Sanhueza, I. A.; Kalvet, I.; Schoenebeck, F. Computational Studies of Synthetically Relevant Homogeneous Organometallic Catalysis Involving Ni, Pd, Ir, and Rh: An Overview of Commonly Employed DFT Methods and Mechanistic Insights. *Chem. Rev.* **2015**, *115* (17), 9532–9586.

(5) Sperger, T.; Sanhueza, I. A.; Schoenebeck, F. Computation and Experiment: A Powerful Combination to Understand and Predict Reactivities. *Acc. Chem. Res.* **2016**, *49* (6), 1311–1319.

(6) Funes-Ardoiz, I.; Schoenebeck, F. Established and Emerging Computational Tools to Study Homogeneous Catalysis—From Quantum Mechanics to Machine Learning. *Chem* **2020**, *6* (8), 1904–1913.

(7) Ahn, S.; Hong, M.; Sundararajan, M.; Ess, D. H.; Baik, M.-H. Design and Optimization of Catalysts Based on Mechanistic Insights Derived from Quantum Chemical Reaction Modeling. *Chem. Rev.* **2019**, *119*, 6509–6560.

(8) Becke, A. D. Density-Functional Thermochemistry. III. The Role of Exact Exchange. *J. Chem. Phys.* **1993**, *98* (7), 5648.

(9) Grimme, S.; Antony, J.; Ehrlich, S.; Krieg, H. A Consistent and Accurate Ab Initio Parametrization of Density Functional Dispersion Correction (DFT-D) for the 94 Elements H-Pu. *J. Chem. Phys.* **2010**, *132* (15), 154104.

(10) Grimme, S.; Ehrlich, S.; Goerigk, L. Effect of the Damping Function in Dispersion Corrected Density Functional Theory. *J. Comput. Chem.* **2011**, *42*, 1456–1465.

(11) Fukui, K. The Path of Chemical Reactions -- The IRC Approach. *Acc. Chem. Res.* **1981**, *14*, 363–368.

(12) Gonzalez, C.; Schlegel, H. B. Reaction Path Following In Mass-Weighted Internal Coordinates Cartesians and with Internal Coordinates without Mass-Weighting. *J. Phys. Chem.* **1990**, *94*, 5523–5527.

(13) Maeda, S.; Harabuchi, Y.; Ono, Y.; Taketsugu, T.; Morokuma, K. Intrinsic Reaction Coordinate: Calculation, Bifurcation, and Automated Search. *Int. J. Quantum Chem.* **2015**, *115*, 258–269.

(14) Bootsma, A. N.; Wheeler, S. E. Popular Integration Grids Can Result in Large Errors in DFT-Computed Free Energies. *ChemRxiv* **2019**, 1–20.

(15) Hariharan, P. C.; Pople, J. A. The Influence of Polarization Functions on Molecular Orbital Hydrogenation Energies. *Theor. Chim. Acta* **1973**, *28* (3), 213–222.

(16) Hay, P. J.; Wadt, W. R. Ab Initio Effective Core Potentials for Molecular Calculations . Potentials for the Transition Metal Atoms Sc to Hg Ab Initio Effective Core Potentials for Molecular Calculations . Potentials for the Transition Metal Atoms Sc to Hg. *J. Chem. Phys.* **1985**, *82*, 270.

(17) Dunning, T. H.; Hay, P. J. Gaussian Basis Sets for Molecular Calculations. In *Methods of Electronic Structure Theory*; Schaefer, H. F., Ed.; Springer: Boston, MA, 1977; pp 1–27.

(18) Hansen, J.; Autschbach, J.; Davies, H. M. L. Computational Study on the Selectivity of Donor/Acceptor-Substituted Rhodium Carbenoids. *J. Org. Chem.* **2009**, *74* (17), 6555–6563.

(19) Papajak, E.; Truhlar, D. G. Efficient Diffuse Basis Sets for Density Functional Theory. *J. Chem. Theory Comput.* **2010**, *6*, 597–601.

(20) Álvarez-Moreno, M.; De Graaf, C.; López, N.; Maseras, F.; Poblet, J. M.; Bo, C. Managing the Computational Chemistry Big Data Problem: The IoChem-BD Platform. *J. Chem. Inf. Model.* **2015**, *55* (1), 95–103.

(21) Fukuto, J. M.; Jensen, F. R. Mechanisms of SE2 Reactions: Emphasis on Organotin Compounds.

Acc. Chem. Res. **1983**, *16* (5), 177–184.
(22) More O'Ferrall, R. A. Relationships between E2 and E1cB Mechanisms of β-Elimination. *J. Chem. Soc. B Phys. Org.* **1970**, 274–277.
(23) Jencks, W. P. General Acid-Base Catalysis of Complex Reactions in Water. *Chem. Rev.* **1972**, *72*, 705–718.
(24) Tantillo, D. J. Recent Excursions to the Borderlands between the Realms of Concerted and Stepwise: Carbocation Cascades in Natural Products Biosynthesis. *J. Phys. Org. Chem.* **2008**, *21* (7–8), 561–570.
(25) Nakamura, E.; Yoshikai, N.; Yamanaka, M. Mechanism of C-H Bond Activation/C-C Bond Formation Reaction between Diazo Compound and Alkane Catalyzed by Dirhodium Tetracarboxylate. *J. Am. Chem. Soc.* **2002**, *124* (24), 7181–7192.
(26) Carpenter, B. K. Energy Disposition in Reactive Intermediates. *Chem. Rev.* **2013**, *113* (9), 7265–7286.
(27) Plata, R. E.; Singleton, D. A. A Case Study of the Mechanism of Alcohol-Mediated Morita Baylis−Hillman Reactions. The Importance of Experimental Observations. *J. Am. Chem. Soc.* **2015**, *137* (11), 3811–3826.
(28) Costil, R.; Sterling, A. J.; Duarte, F.; Clayden, J. Atropisomerism in Diarylamines: Structural Requirements and Mechanisms of Conformational Interconversion. *Angew. Chemie - Int. Ed.* **2020**, *59* (42), 18670–18678.
(29) The consistency between theory and experiment, however, could emerge for the following reasons. (1) Getting the right answers for the right reasons—our truncated model and choice of theoretical method are sufficient in capturing the key interactions between the chiral cavity and its substrate, which lead to the observed dr and er, and our energies provide an adequate model for these observed ratios. (2) Getting the right answers for the wrong reasons: even with cancellation of error in DFT methods, we happened to stumble upon matches with experiment for *R*-catalyst, in which case we have proposed a preliminary model that happens to match experiment but does not accurately reflect reality at the molecular level. (3) Finally, alternative mechanistic possibilities converge to the same set of experimental data: the ratio of stereoisomers being formed that emerge is indeed consistent with the energies computed here, however, something else is occurring that we cannot capture with the current stationary-point analysis (a "thin" approach to mechanism). If this is the case, a "thicker" mechanistic picture would be required, which might look something like (but no means limited to) an *ab initio* molecular dynamics (AIMD) study or a study in a box of explicit solvent, both of which are intractable with our current modeling capabilities. The proposed mechanism here hinges on whether the level of theory used accurately captures key interactions giving rise to the computed activation barriers, crucial for predicted selectivities, and whether our "thin" mechanism did not miss something altogether, like a change in ligand orientation, a dynamic effect, or a solvent effect. As we found in our exploratory studies on the performance of various DFT functionals, any one functional resulted in qualitatively different major product predictions (that is, if transition-state theory is a valid and applicable model). Nevertheless, our mechanism lays the groundwork for future mechanistic explorations of such a (in the authors' opinion) mind-bending reaction where non-trivial factors govern observed selectivity.